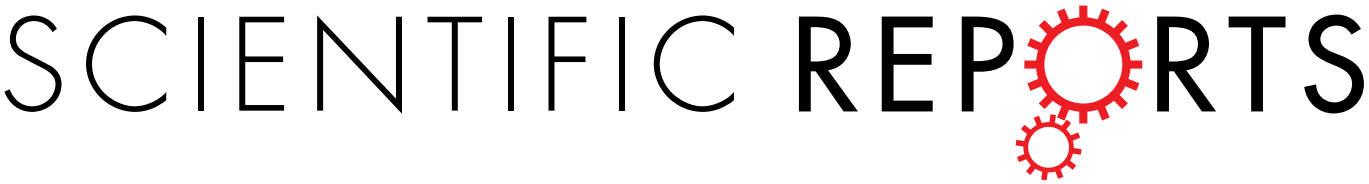

OPEN

Mechano-adaptive sensory mechanism of α-catenin under tension

Received: 09 December 2015
Accepted: 07 April 2016
Published: 25 April 2016

Koichiro Maki[1,2], Sung-Woong Han[3], Yoshinori Hirano[4], Shigenobu Yonemura[5], Toshio Hakoshima[4] & Taiji Adachi[1,2]

The contractile forces in individual cells drive the tissue processes, such as morphogenesis and wound healing, and maintain tissue integrity. In these processes, α-catenin molecule acts as a tension sensor at cadherin-based adherens junctions (AJs), accelerating the positive feedback of intercellular tension. Under tension, α-catenin is activated to recruit vinculin, which recruits actin filaments to AJs. In this study, we revealed how α-catenin retains its activated state while avoiding unfolding under tension. Using single-molecule force spectroscopy employing atomic force microscopy (AFM), we found that mechanically activated α-catenin fragment had higher mechanical stability than a non-activated fragment. The results of our experiments using mutated and segmented fragments showed that the key intramolecular interactions acted as a conformational switch. We also found that the conformation of α-catenin was reinforced by vinculin binding. We demonstrate that α-catenin adaptively changes its conformation under tension to a stable intermediate state, binds to vinculin, and finally settles into a more stable state reinforced by vinculin binding. Our data suggest that the plastic characteristics of α-catenin, revealed in response to both mechanical and biochemical cues, enable the functional-structural dynamics at the cellular and tissue levels.

A combination of contractile forces in individual cells drives tissue dynamics such as morphogenesis[1–3] and wound healing[4]. The cadherin-based adherens junctions (AJs) function as direct links between the contractile actomyosin cytoskeletons of different cells[5,6]. AJs balance the intercellular tensions by the adaptive assembly of the cytoskeletal actin filaments[7–10]. In this mechano-adaptive mechanism, α-catenin, a tension-sensing component of AJs, is critical regulator of vinculin binding[11–13], which recruits another actin filament to AJ[14,15].

The molecular mechanisms of the regulation of vinculin binding by α-catenin have been investigated using various approaches. The molecular and cellular study of Yonemura *et al.*[16] has revealed that α-catenin under intercellular tension exposes the cryptic vinculin binding site (VBS). The process is triggered by the release of the autoinhibited conformation caused by an intramolecular interaction between its M_I domain (residues 275–391) containing VBS (residues 325–360) and the vinculin-inhibitory M_{II}–M_{III} domain (residues 510–697). The autoinhibited conformation has been determined in the crystallized α-catenin [PDB code: 4K1N][17], where the vinculin-binding surface of VBS is buried in the helix bundle of M_I domain that is structurally stabilized by M_{II}–M_{III} helix bundles. Single-molecule experiments using magnetic tweezers have suggested that the disruption of M_I/M_{II}–M_{III} interaction requires only approximately 5-pN tension[18], which is close to the range of forces generated by a single myosin molecule[19]. Thereby, the M_I/M_{II}–M_{III} interaction holds the key to the mechanical activation of α-catenin, recruiting vinculin under tension.

However, α-catenin mechanically activated under tension faces a critical problem common to all tension-sensing proteins. Usually, an external force acts as a biomolecule denaturant[20,21]. A study[22] using atomic force microscopy (AFM) has reported a complete unfolding of a protein in approximately 30 s under low tension

[1]Department of Biomechanics, Institute for Frontier Medical Sciences, Kyoto University, 53 Shogoin-Kawahara-cho, Sakyo, Kyoto 606-8507, Japan. [2]Department of Micro Engineering, Graduate School of Engineering, Kyoto University, Yoshida Honmachi, Sakyo, Kyoto 606-8501, Japan. [3]National Institute for Nanomaterials Technology, Pohang University of Science and Technology, 77 Cheongam-ro, Nam-Gu, Pohang, Gyeongbuk 790-784, Korea. [4]Structural Biology Laboratory, Graduate School of Biological Sciences, Nara Institute of Science and Technology, 8916-5 Takayama, Ikoma, Nara 630-0192, Japan. [5]Ultrastructural Research Team, RIKEN Center for Life Science Technologies, 2-2-3 Minatojima-minamimachi, Chuo-ku, Kobe, Hyogo 650-0047, Japan. Correspondence and requests for materials should be addressed to T.A. (email: adachi@frontier.kyoto-u.ac.jp)

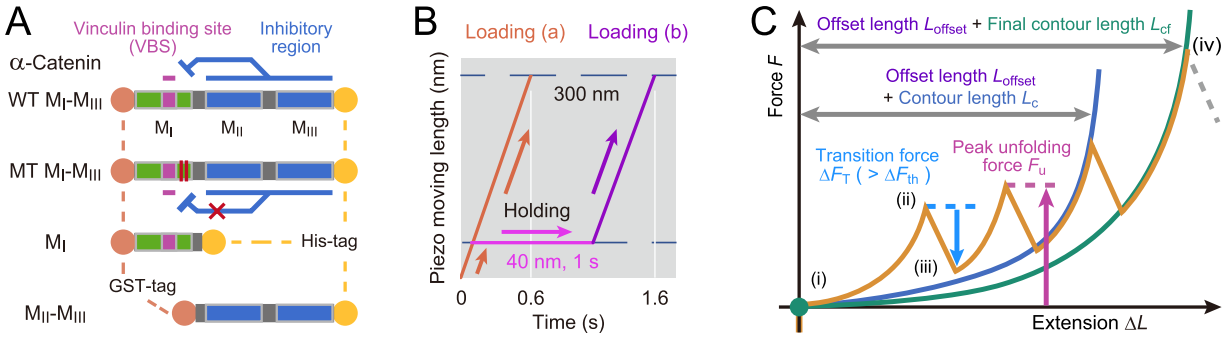

Figure 1. SMFS using AFM. (**A**) α-Catenin fragments: WT M_I-M_{III} (residues 276–634), mutant (MT) M_I-M_{III} (M319G and R326E), M_I (residues 276–393), and M_{II}–M_{III} (residues 385–634). (**B**) Loading conditions (a) and (b). Single α-catenin molecules were loaded by NanoWizard 3 BioAFM (JPK Instruments, Berlin, Germany). The piezo-actuator was moved upward by 300 nm at a constant speed of 500 nm/s ("Loading (a)" in this study, orange line). To analyze the mechanical behavior of WT M_I-M_{III} after mechanical activation, we introduced a holding time of 1 s at 40 nm of constant piezo-moving length ("Loading (b)," orange (initial loading), magenta (holding), and purple (further loading)). (**C**) Force curve analysis. First, the force curves with saw-tooth patterns (state (i) to (iv), orange curve) caused by single-molecule behaviors were identified, with the rupture force and final stiffness in the last peak (state (iv)). Next, the offset length L_{offset} was determined by WLC-model fitting to the last peak (green curve) with the fixed final contour length L_{cf} (143.2 nm (WT/MT M_I-M_{III}), 46.8 nm (M_I), and 99.6 nm (M_{II}–M_{III})). Finally, we measured the contour length L_c and peak unfolding force F_u at each force peak with transition force ΔF_T (state (ii) to (iii)) greater than the threshold ΔF_{th} (Methods: "Force curve analysis").

of approximately 13 pN. Furthermore, α-helical proteins such as α-catenin have lower mechanical stabilities than other β-sheet proteins[23]. During the tension-sensing process, the helical conformation of VBS should be conserved to associate with vinculin[24]. Thus, the most significant question is how does α-catenin, one of the tension-sensing proteins, retain its activated state while avoiding the successive unfolding under denaturing tension.

Here, we revealed that α-catenin under tension changed its conformation to a stable intermediate state. We investigated the mechanical behaviors of mutated, segmented, and vinculin-bound α-catenin using single-molecule force spectroscopy (SMFS)[25–27] employing AFM. To reveal the conformational changes in α-catenin under tension, we adopted the following two types of loading conditions: (a) direct loading without mechanical activation and (b) loading with a holding period to wait for mechanical activation.

Results

Mechano-adaptive conformational change in M_I-M_{III}. We used four types of α-catenin fragments (Fig. 1A): wild type (WT) M_I-M_{III} (residues 276–634), mutant (MT) M_I-M_{III} (M319G and R326E), M_I (residues 276–393), and M_{II}–M_{III} (residues 385–634). The mutant fragment, in which the autoinhibiting MI/M_{II}–M_{III} interaction is disrupted, behaved as an activated α-catenin that interacts with vinculin under no tension (Supplementary Figure 1). The weakened M_I/M_{II}–M_{III} interaction causes a change in the angle between helix bundles M_{II} and M_{III}[17] and the destabilization of helix bundle M_I[28]. α-Catenin fragments bound to the glass substrate at the C-terminus exploiting NTA-Ni^{2+}-His_6 affinity were loaded at the N-terminus using GST-GSH affinity. The autoinhibitory WT M_I-M_{III} fragment was examined in the following two types of loading conditions (Fig. 1B): (a) direct loading (orange line) and (b) loading with a holding period (magenta line) to wait for mechanical activation. The force curves corresponding to the single α-catenin molecules were extracted and their characteristics were analyzed (Fig. 1C); we calculated contour length L_c to identify intermediate states during unfolding and the measured peak unfolding force F_u to estimate the mechanical stabilities of the abovementioned α-catenin fragments.

WT M_I-M_{III} fragment in loading (a) unfolded each domain under tension. To analyze the stochastic unfolding trajectories from obtained force curves (Fig. 2A), we evaluated the number density of force peaks, n_d (L_c, F_u) on the basis of scatter plots of F_u versus L_c. The contour map of the number density n_d showed three wide horizontal regions with similar intervals (Fig. 2B; the contour map with regard to net extension is shown in Supplementary Figure 2A). The low n_d in the initial region (green line) indicated that the weak helix bundle of M_I unfolded easily, with infrequent force peaks. However, the last two regions (blue lines) with high n_d, i.e., with frequent force peaks, corresponded to two stable helix bundles of M_{II}–M_{III} domain. These results indicated that M_I-M_{III} domain unfolding depended on the mechanical stability of their helix bundles under direct loading.

However, WT M_I-M_{III} in loading (b) showed force peaks within a rather greater force range (Fig. 2C), and the contour map of n_d showed greater peak unfolding force F_u (Fig. 2D) than those in loading (a) (Fig. 2B). This result indicated that the conformation of M_I-M_{III} domain changed to another intermediate state that required higher tension for further unfolding. As the peak unfolding force F_u increased along the entire contour length L_c (Fig. 2D), the conformational change must have occurred at all three M_I-M_{III} domains. The contour map showed a specific peak at L_c of approximately 45.4 nm (arrow, Fig. 2D); the net extension was approximately 19.0 nm

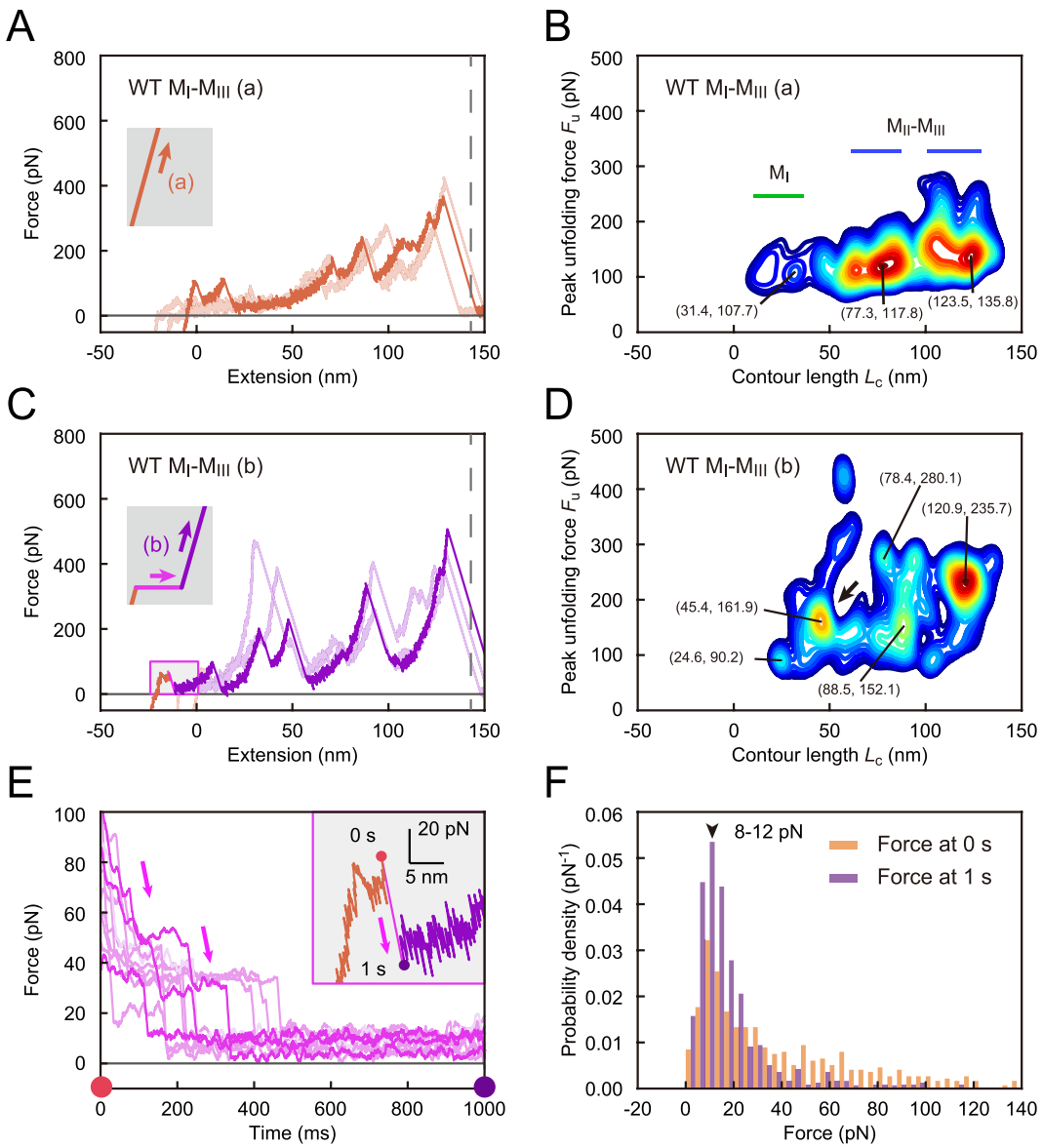

Figure 2. Conformational change in M_I-M_{III} domain under tension. (**A**) Force curves for WT M_I-M_{III} fragment in loading (a). The force curves are shifted to the left by the offset length L_{offset}. (**B**) Contour map of number density n_d of force peaks in loading (a) based on 797 force curves. Color contours are set from the maximum value of n_d (red) to 0.4 × the value (blue). (**C**) Force curves in loading (b). (**D**) Contour map in loading (b) based on 514 force curves. (**E**) Force relaxation curve during the holding time. (**F**) The probability density of force at 0 s (orange bars) and 1 s (purple bars) during the holding time.

(Supplementary Figure 2B), <40% of completely extended length of M_I domain. This observation suggested that VBS in M_I domain was conserved in this region. During the holding time, the force relaxation curve showed stepwise relaxations (Fig. 2E), implying dynamic transitions in the M_I-M_{III} conformation. The force distribution at the beginning (0 s) of the holding time settled into a narrow distribution approximately 10 pN at the end of this period (1 s, Fig. 2F), showing that the M_I-M_{III} conformation finally equilibrated under low tension. We suggest that M_I/M_{II}–M_{III} interaction was partly diminished during the holding time; the average extension of approximately 2.8 nm in the holding period was longer than the reported extension[28] that was approximately 1.0 nm for the mechanical activation of M_I-M_{III} domain. The probability density of the force peaks in loading (b) in the initial extension was lower than that in loading (a), which supported this suggestion (Supplementary Figure 2C). Thus, we revealed that M_I-M_{III} domain of α-catenin adaptively changes the conformation to another stable state under low tension, with weakened M_I/M_{II}–M_{III} interaction.

M_I/M_{II}–M_{III} interaction as a conformational switch. To elucidate the conformational changes in the M_I-M_{III} domain with weakened M_I/M_{II}–M_{III} interaction, we examined the MT M_I-M_{III} fragment (force curves are shown in Supplementary Figure 3A). The contour map for MT M_I-M_{III} showed two specific regions (L_c = 19.4 nm

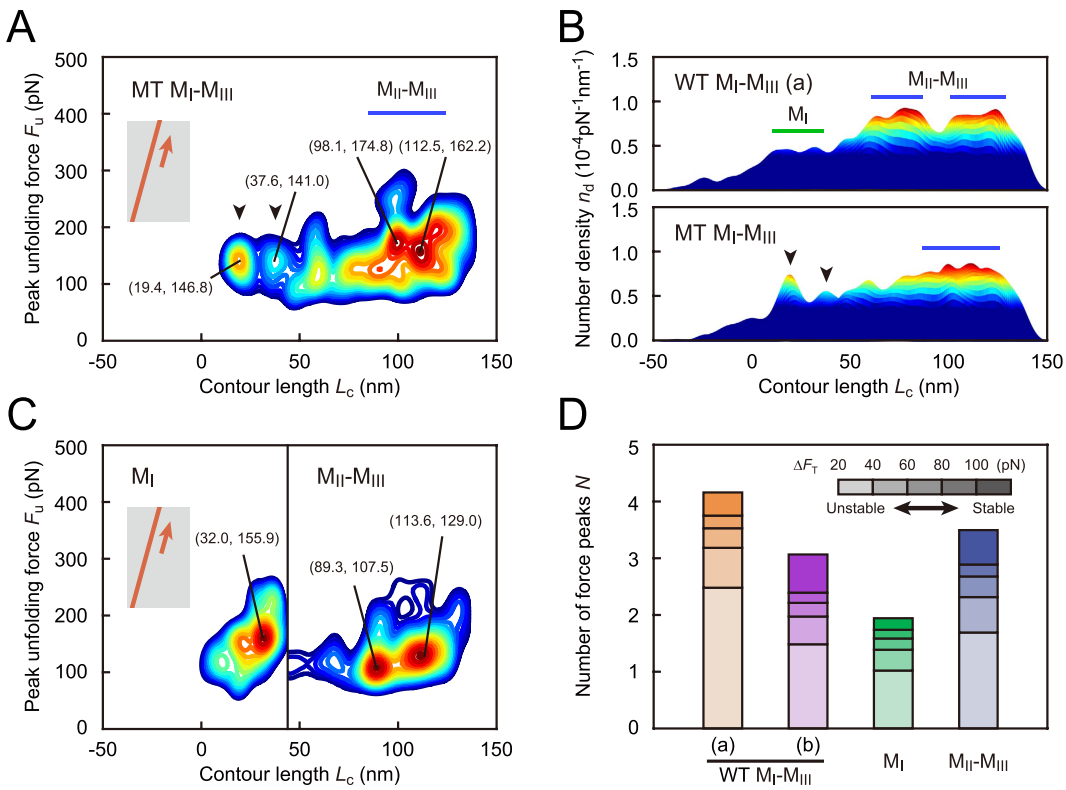

Figure 3. Mechanical behaviors of mutated and segmented α-catenin. (**A**) Contour map for MT M_I-M_{III} fragment based on 576 force curves. (**B**) Comparison of the number density n_d in contour maps from a side view in WT and MT M_I-M_{III} fragments. (**C**) Contour maps for M_I and M_{II}–M_{III} fragments based on 181 and 785 force curves, respectively. The contour map for M_{II}–M_{III} fragment is shifted to the right by 46.8 nm, which corresponds to the fully-extended length of M_I domain. (**D**) The average number of force peaks N per curve. The stacked bar graphs display N values, with color intensity illustrating the range of transition force ΔF_T. The substructure stability increases with the increasing ΔF_T values.

and 37.6 nm, arrowheads in Fig. 3A; the contour map with regard to net extension is shown in Supplementary Figure 3B). The regions had greater peak unfolding forces F_u (146.8 pN and 141.0 pN) than those for WT in loading (a) (Fig. 2B). Moreover, the number densities n_d in these regions were higher than those in WT (arrowheads, the side view of n_d distribution in Fig. 3B). Furthermore, in the later region (50 nm $< L_c <$ 150 nm), two separate regions observed in WT M_I-M_{III} (blue lines, upper part of Fig. 3B) fused into one broad region in MT (lower part of Fig. 3B). This observation indicated that M_{II}–M_{III} domain changed its conformation because of weakened M_I/M_{II}–M_{III} interaction. The result for MT M_I-M_{III} indicated that weakened M_I/M_{II}–M_{III} interaction triggers the changes in M_I-M_{III} conformation.

Individual M_I and M_{II}–M_{III} fragments showed one and two regions, respectively (Fig. 3C; force curves are shown in Supplementary Figure 3C,D) with higher n_d values (Supplementary Figure 3E) than those for M_I-M_{III} fragments, indicating that M_I and M_{II}–M_{III} domains settled into an innate stable state without interacting with each other. In particular, the peak unfolding force for the M_I domain (155.9 pN, Fig. 3C) was approximately 50% greater than that for the corresponding region of WT M_I-M_{III} in loading (a) (107.7 pN, Fig. 2B). This result indicated that the weak helix bundle of M_I changed the conformation to another state with higher mechanical stability without the interaction with M_{II}–M_{III} domain.

To compare the mechanical stabilities of α-catenin fragments, we analyzed the number of force peaks N per curve, as shown in Fig. 3D. The stacked bar graphs (Fig. 3D) display N values, with color intensity illustrating the range of transition force ΔF_T for force peaks (Fig. 1C). The greater ΔF_T values correspond to more stable substructures. For WT M_I-M_{III} fragment (orange and purple bars, Fig. 3D), N values at large ΔF_T (>100 pN, associated with a stable substructure) increased in loading (b) compared with that in loading (a). On the other hand, the value of N at small ΔF_T (20 pN to 40 pN, associated with unstable substructure) decreased in loading (b). This result supported our idea that the conformation of WT M_I-M_{III} changed to a more stable state with weakened M_I/M_{II}–M_{III} interaction under tension. In addition, the sum of the N values for M_I (green bar, Fig. 3D) and M_{II}–M_{III} (blue bar) was greater than that for WT M_I-M_{III} in loading (a). This result suggested that the M_I/M_{II}–M_{III} interaction destabilized the M_I and M_{II}–M_{III} conformations under no force. On the basis of the results for mutated and segmented α-catenin fragments, we determined that the M_I/M_{II}–M_{III} interaction acted as an intramolecular switch to induce the mechano-adaptive conformational change of M_I-M_{III} domain.

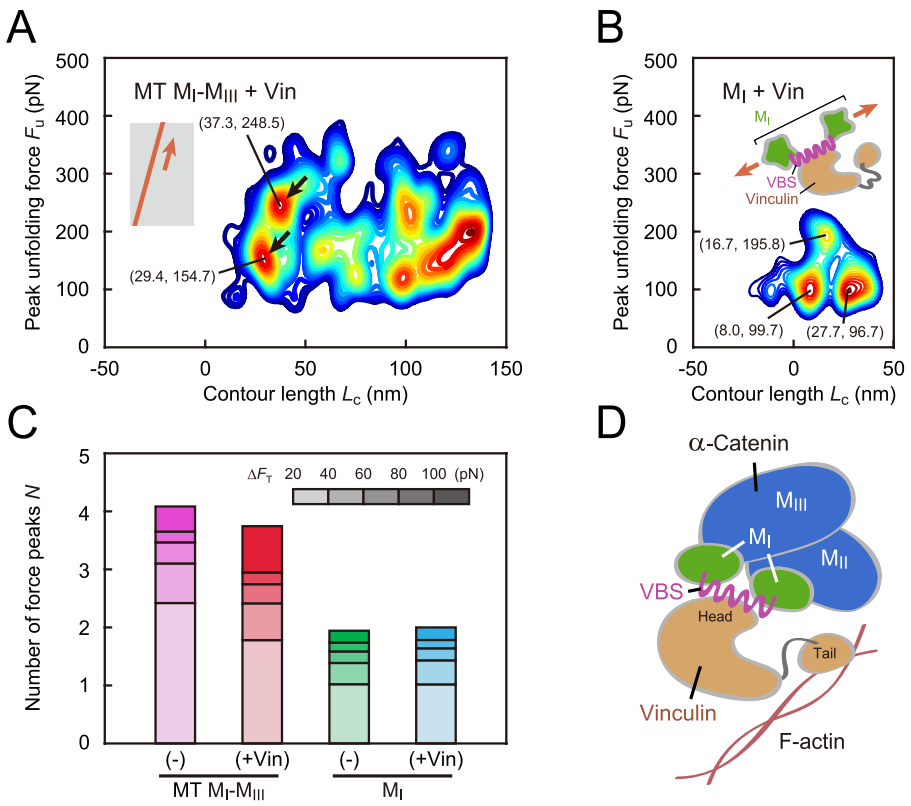

Figure 4. The effect of vinculin binding on mechanical behavior of α-catenin. (**A**) Contour map for vinculin-bound MT M_I-M_{III} fragment based on 571 force curves. (**B**) Contour map for vinculin-bound M_I fragment based on 111 force curves. The conformation of vinculin-bound M_I domain comprised a stable helix of VBS with high F_u and two unstable substructures with low F_u. (**C**) Changes in the average number of force peaks N caused by vinculin binding. (**D**) Schematic of the molecular complex consisting of α-catenin, vinculin, and actin filament (F-actin). M_I-M_{III} domain was reinforced by vinculin binding at the head domain, in which the M_{II}–M_{III} domain stabilized the conformation of vinculin-bound M_I domain. The tail domain of vinculin associates with another actin filament.

Reinforcing vinculin binding to M_I-M_{III}. To elucidate how the vinculin binding affects the mechanical behavior of α-catenin, we examined the α-catenin fragments after vinculin treatment. Vinculin binds to an α-catenin molecule with the head domain, and the tail domain associates with another actin filament. The contour map of n_d for vinculin-bound MT M_I-M_{III} showed characteristic regions ($L_c = 29.4$ nm and 37.3 nm; arrows in Fig. 4A; force curves are shown in Supplementary Figure 4A) at a greater peak unfolding force F_u (154.7 pN and 248.5 pN) than that for MT M_I-M_{III} without vinculin (Fig. 3A). This result indicated that M_I-M_{III} domain was reinforced by vinculin binding. In contrast to MT M_I-M_{III}, vinculin-bound M_I (Fig. 4B; force curves are shown in Supplementary Figure 4B) showed two regions at smaller F_u (99.7 pN and 96.7 pN) than M_I without vinculin (155.9 pN, Fig. 3C). Vinculin-bound M_I showed one region at a rather greater F_u (195.8 pN, Fig. 4B). This result indicated that the conformation of vinculin-bound M_I comprised a stable helix of VBS and two unstable substructures remaining in this domain.

Comparing the results for MT M_I-M_{III} and M_I fragments, we concluded that the M_{II}–M_{III} domain stabilized the unstable vinculin-bound M_I domain. Thus, the number of force peaks N at large ΔF_T (>100 pN) for MT M_I-M_{III} was increased by vinculin binding (red bar, Fig. 4C), with a decrease in N at small ΔF_T (20 pN–40 pN). The number of force peaks for M_I did not change significantly (cyan bar, Fig. 4C). The stabilizing role of M_{II}–M_{III} domain was further confirmed in the analysis of total energy E_{tot} for completely unfolding (Supplementary Figure 5). E_{tot} for M_I decreased after vinculin binding (cyan bar) that was caused by greater decrease in unfolding energy for two unstable substructures than the increase in unfolding energy for stable VBS helix. However, MT M_I-M_{III} increased after vinculin binding (red bar). The results for vinculin-bound α-catenin fragments revealed that M_I-M_{III} domain was reinforced by vinculin binding at the head domain (Fig. 4D), with M_{II}–M_{III} domain stabilizing the conformation of the vinculin-bound M_I.

Changes in the persistence length of M_I-M_{III} as a polymer chain. To examine the changes in the α-catenin molecule as a polymer chain, we analyzed the persistence length l_p (Fig. 5A). In the initial extension ($0\,\text{nm} < L_c \leq 72\,\text{nm}$, the left plot in Fig. 5A), the persistence length l_p for WT M_I-M_{III} in loading (b) (purple bar) was greater than in loading (a) (orange bar). This result indicated that the persistence length was increased by mechanical activation, resulting in the decreased tensile force required to a certain amount of extension (Fig. 5B). No significant differences were observed in the later extension ($72\,\text{nm} < L_c < 144\,\text{nm}$, the right plot in Fig. 5A).

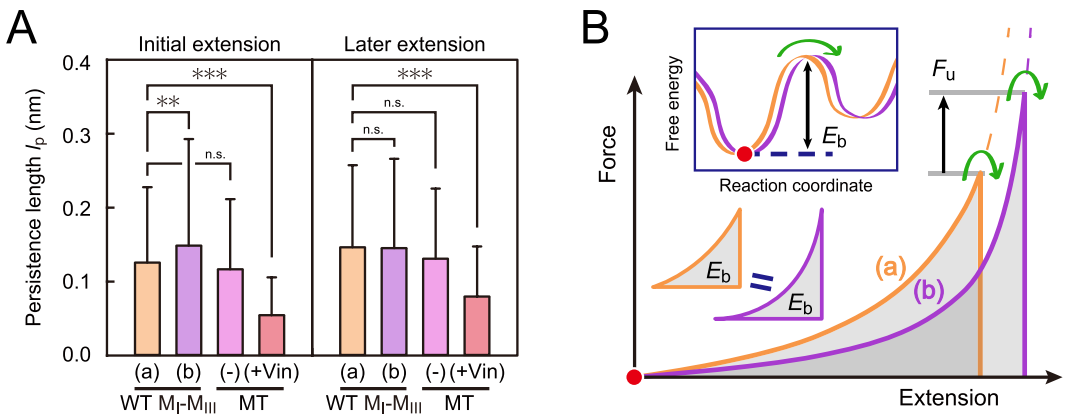

Figure 5. Changes in the persistence length of α-catenin as a polymer chain. (**A**) Comparison of persistence lengths l_p in M_I-M_{III} fragments. Statistical significance of the differences was analyzed using *t*-test ($^{**}p < 0.01$ and $^{***}p < 0.005$). The error bars show standard deviations (S.D.). Persistence length l_p was analyzed in the initial extension ($0\,nm < L_c \leq 72\,nm$) and the later extension ($72\,nm < L_c < 144\,nm$). (**B**) The effect of persistence length on the peak unfolding force. If we postulate the same energy barrier E_b for the next intermediate state in M_I-M_{III} before and after the activation (orange (a) and purple (b) lines), greater peak unfolding force F_u will be required to overcome the E_b in the activated M_I-M_{III} (b), with greater l_p, than in M_I-M_{III} (a).

After vinculin binding, l_p settled to a much smaller value in the entire extension (red bars in Fig. 5A), indicating that the M_I-M_{III} domain was immobilized because of the conformational reinforcement caused by vinculin.

Here, the increase in l_p of M_I-M_{III} by mechanical activation was consistent with the increase in the peak unfolding force F_u. We can postulate the same energy barrier E_b for the next intermediate state in M_I-M_{III} before and after the activation (Fig. 5B) on the basis of the total unfolding energy E_{tot} (Supplementary Figure 5). Further, the activated M_I-M_{III} (b), with greater l_p, should be extended more to overcome the energy barrier E_b than M_I-M_{III} (a), with smaller l_p, resulting in a greater peak unfolding force F_u. Thus, the M_I-M_{III} domain of α-catenin under tension changes the conformation to an intermediate state with a larger persistence length, and finally settles into the immobilized state caused by the reinforcement with vinculin.

Discussion

On the basis of our single-molecule experiments, we revealed the mechano-adaptive sensory mechanism of α-catenin. Under physiologically possible low tension, α-catenin adaptively changed the conformation to a stable intermediate state. Such mechano-adaptive conformational changes enable α-catenin at AJs to retain the activated state under tension, without successive unfolding, to function as a robust tension sensor. Our findings could be one solution to a paradox. The tension-sensing proteins require mechanical forces for their activation; however, they have to be stable under such conditions because the mechanical forces function as basic protein denaturants. Furthermore, we revealed that vinculin-binding reinforces α-catenin conformation; the stable α-catenin-vinculin complex contributes to the tight anchoring of adhesive molecules at AJs[29] by recruiting another actin filament. Therefore, we suggest that the mechano-adaptive sensory ability of α-catenin arises from its molecular plasticity in response to both mechanical and biochemical cues.

Our results for mutated (MT M_I-M_{III}) and segmented (M_I, M_{II}–M_{III}) α-catenin reveal that the M_I/M_{II}–M_{III} interaction acts as a conformational switch to the intermediate state, where M_I and M_{II}–M_{III} domains change to the conformations with increased stability. Our results are consistent with the previous reports that the helix bundle of M_I requires the structural stabilization by M_{II}–M_{III}[28] and that helix bundles M_{II}–M_{III} are approximately 180°-rotated in conformation without M_I domain[30,31]. However, there were some discrepancies between the results for MT M_I-M_{III} without mechanical activation and those for WT M_I-M_{III} in loading (b) with mechanical activation. Thus, we should consider both the importance of tension for the drastic conformational changes and the conformational switch caused by M_I/M_{II}–M_{III} interaction.

In our experiments, the full-length vinculin firmly bound to MT M_I-M_{III} fragment, with an increase in peak unfolding force F_u and a decrease in the persistence length l_p. The full-length vinculin assumes an autoinhibited conformation for α-catenin-binding[32]. Our results suggested that the VBS exposed in the mechanically-activated α-catenin opens the autoinhibited conformation of vinculin to make a stable α-catenin–vinculin complex. Our data supported the previous reports[24,33] that α-catenin and vinculin are "co-activated" for interacting with each other under tension. This type of a force-induced vinculin-activation mechanism of α-catenin could be conserved in talin and α-actinin that are similar adhesive proteins constituting a molecular complex with vinculin and actin filament[34].

The loading rate used here was appropriate for the qualitative analysis of the mechanical behavior of α-catenin. Our results for WT M_I-M_{III} in loading (a) were in agreement with the results of the experiments (performed using magnetic tweezers) using a low loading rate (approximately 4 pN/s)[18]. Moreover, the "holding" method utilized in our study allowed us to analyze the conformational changes under physiologically possible low tension of approximately 10 pN. Thus, by introducing the holding time into fast loadings, we succeeded in analyzing the

conformational changes of α-catenin molecules under low tension while efficiently exploring their unfolding trajectories.

The persistence length L_p appeared in this study was smaller than that reported (approximately 0.4 nm) for titin molecules[35]. This discrepancy may be related to the secondary structures of molecules. A previous study[36] employing molecular dynamics simulation revealed that a protein with high φ dihedral potential shows a small persistence length of 0.19 nm. This suggests that α-helical proteins such as α-catenin, of which φ dihedral angle is more constrained than β-sheet proteins such as titin, exhibit smaller persistence length. In addition, subcomponents in α-catenin molecules, such as helix bundles, could decrease the persistence length L_p.

Based on our study, we propose a novel concept of "mechano-adaptive" molecules that fulfill their innate functions by adapting to the cellular forces. Under these forces, biomolecules such as proteins and nucleic acids may change their conformations, mechanical behaviors, and chemical properties. Such molecular-scale changes under mechanical forces could affect force-induced phenomena at cellular and tissue level. We believe that our study may be the basis for future studies investigating the concept of mechano-adaptive sensory mechanism.

Methods

Protein purification. DNA fragments of mouse WT αE-catenin M_I-M_{III}, MT M_I-M_{III}, M_I, and M_{II}–M_{III} were amplified by PCR and cloned into the pGEX6P-3 vector (GE Healthcare). All plasmids were verified by DNA sequencing and transformed into *Escherichia coli* strain BL21Star (DE3) (Invitrogen) cells for protein expression. Protein expression was performed at 20 °C in Luria–Bertani medium containing 0.1 mM isopropyl-β-D-thiogalactopyranoside. Cells expressing αE-catenin were suspended in 20 mM Tris-HCl buffer (pH 8.0) containing 150 mM NaCl and disrupted by sonication. After ultracentrifugation, the supernatant was applied onto a Glutathione Sepharose 4B column (GE Healthcare). Eluted proteins were further purified by anion-exchange (HiTrap Q HP, GE Healthcare) and gel filtration (Superdex 200 pg, GE Healthcare) chromatography.

Chemical modification. For SMFS, a glass substrate and AFM tip were treated using a chemical modification process[21]. The glass substrate was modified with α-catenin at its C-terminus and AFM tip was modified with glutathione, which interacts with N-terminal GST-tag of α-catenin. The glass substrate was oxidized and treated with 2% MPTMS/ethanol for 15 min. The substrate was then treated with 2 mM maleimide-C_3-NTA (Mal-C_3-NTA; DOJINDO Lab.)/PBS for 30 min, with 10 mM $NiCl_2$ (Wako Pure Chemical Industries)/Milli-Q for 30 min, and washed with PBS. α-Catenin fragments (10 μM for each fragment) were modified by NTA-Ni^{2+}-His_6 affinity binding for 1 h and finally washed with working buffer (10 mM HEPES, 150 mM NaCl, pH 7.2). For the SMFS of vinculin-bound α-catenin fragments, the α-catenin-modified substrate was further incubated with 1 μM full-length vinculin/PBS for 30 min and washed with working buffer. Silicon nitride AFM tip (OMCL-TR400PSA-1; spring constant, 0.02 N/m, Olympus Co.) was first oxidized using ozone cleaner and treated with 2% APTES/ethanol for 15 min. The tip was then treated with 1.5 mM Mal-PEG-NHS ester/PBS for 30 min and with 10 mM glutathione/PBS for 1 h. The remaining maleimide was quenched with 50 mM 2-mercaptoethanol/HEPES and finally washed with working buffer.

Force curve analysis. Force curves with saw-tooth peaks, caused by conformational transitions of α-catenin, were analyzed using the in-house software (Fig. 1C). First, we extracted the force curves for completely extended single α-catenin molecules, based on the thresholds of force and stiffness at the rupture event, assuming an 85%-extended worm-like chain model[37],

$$F(\Delta L) = \frac{k_B T}{l_{pf}}\left[\frac{1}{4}\left(1 - \frac{\Delta L}{L_{cf}}\right)^{-2} + \frac{\Delta L}{L_{cf}} - \frac{1}{4}\right], \tag{1}$$

where k_B is the Boltzmann constant, T is temperature [300 K], l_{pf} is the final persistence length [0.4 nm] based on a previous report[35]. The final contour length L_{cf} was estimated as 143.2 nm (WT/MT M_I-M_{III}), 46.8 nm (M_I), and 99.6 nm (M_{II}–M_{III}) based on the number of residues. The threshold of the stiffness excluded the curves with low stiffness for aggregated molecules. For the extracted curves, we determined the length of offset L_{offset}, corresponding to PEG length (approximately 45 nm) and the tip curvature radius, by fitting WLC model allowing baseline offset as

$$F(\Delta L) = \frac{k_B T}{l_{pf}}\left[\frac{1}{4}\left(1 - \frac{\Delta L}{L_{cf} + L_{offset}}\right)^{-2} + \frac{\Delta L}{L_{cf} + L_{offset}} - \frac{1}{4}\right], \tag{2}$$

to the final peak at the rupture event (green line, Fig. 1C), where L_{offset} was a fitting parameter. Finally, we identified the intermediate force peaks with the transition force ΔF_T (cyan arrow, Fig. 1C) based on the threshold ΔF_{th} (40 pN) and calculated the contour length L_c and the persistence length l_p by fitting WLC model with the determined L_{offset} to the force peaks as

$$F(\Delta L) = \frac{k_B T}{l_p}\left[\frac{1}{4}\left(1 - \frac{\Delta L}{L_c + L_{offset}}\right)^{-2} + \frac{\Delta L}{L_c + L_{offset}} - \frac{1}{4}\right], \tag{3}$$

by considering that the PEG linker, without any substructures, can be fully unfolded at each intermediate state. To analyze the mechanical stabilities for intermediate states, we measured peak unfolding force F_u (magenta arrow, Fig. 1C). We adopted lower ΔF_{th} (20 pN) to detect the force peaks caused by unfolding of unstable substructures.

Number density of force peaks. Based on scatter plots of peak unfolding force F_u versus contour length L_c, we evaluated the number density $n_d(L_c, F_u)$ of force peaks per curve by taking the product of the average number of force peaks per one curve N and the probability density $P(L_c, F_u)$ calculated using two-variable Gaussian distribution function as

$$P(L_c,\ F_u) = \frac{\sum_k g(L_c,\ F_u, L_{ck}, F_{uk})}{\sum_k \left[\iint g(L_c, F_u, L_{ck}, F_{uk}) dL_c dF_u\right]}, \tag{4}$$

where

$$g = \frac{1}{2\pi\sigma_L\sigma_F} \exp\left\{-\frac{1}{2}\left[\frac{(L_c - L_{ck})^2}{\sigma_L^{\ 2}} + \frac{(F_u - F_{uk})^2}{\sigma_F^{\ 2}}\right]\right\}, \tag{5}$$

in which the summation for k meant the summation for all scattered data points.

References

1. Martin, A. C., Gelbart, M., Fernandez-Gonzalez, R., Kaschube, M. & Wieschaus, E. F. Integration of contractile forces during tissue invagination. *J. Cell Biol.* **188,** 735–749 (2010).
2. Eiraku, M. *et al.* Self-organizing optic-cup morphogenesis in three-dimensional culture. *Nature* **472,** 51–56 (2011).
3. Lecuit, T., Lenne, P.-F. & Munro, E. Force generation, transmission, and integration during cell and tissue morphogenesis. *Annu. Rev. Cell Dev. Biol.* **27,** 157–184 (2011).
4. Tamada, M., Perez, T. D., Nelson, W. J. & Sheetz, M. P. Two distinct modes of myosin assembly and dynamics during epithelial wound closure. *J. Cell Biol.* **176,** 27–33 (2007).
5. Harris, T. J. C. & Tepass, U. Adherens junctions: from molecules to morphogenesis. *Nat. Rev. Mol. Cell Biol.* **11,** 502–514 (2010).
6. Meng, W. & Takeichi, M. Adherens junction: molecular architecture and regulation. *Cold Spring Harb. Perspect. Biol.* **1,** a002899; doi: 10.1101/cshperspect.a002899 (2009).
7. Miyake, Y. *et al.* Actomyosin tension is required for correct recruitment of adherens junction components and zonula occludens formation. *Exp. Cell Res.* **312,** 1637–1650 (2006).
8. Levayer, R. & Lecuit, T. Oscillation and polarity of E-cadherin asymmetries control actomyosin flow patterns during morphogenesis. *Dev. Cell* **26,** 162–175 (2013).
9. Engl, W., Arasi, B., Yap, L. L., Thiery, J. P. & Viasnoff, V. Actin dynamics modulate mechanosensitive immobilization of E-cadherin at adherens junctions. *Nat. Cell Biol.* **16,** 584–591 (2014).
10. Sato, K., Ogawa, Y., Ito, S., Fujisawa, S. & Minami, K. Strain magnitude dependent intracellular calcium signaling response to uniaxial stretch in osteoblastic cells. *J. Biomech. Sci. Eng.* **10,** 15–00242; doi: 10.1299/jbse.15-00242 (2015).
11. Lecuit, T. α-Catenin mechanosensing for adherens junctions. *Nat. Cell Biol.* **12,** 522–524 (2010).
12. Yonemura, S. A mechanism of mechanotransduction at the cell-cell interface: emergence of α-catenin as the center of a force-balancing mechanism for morphogenesis in multicellular organisms. *Bioessays* **33,** 732–736 (2011).
13. Kim, T.-J. *et al.* Dynamic visualization of α-catenin reveals rapid, reversible conformation switching between tension states. *Curr. Biol.* **25,** 218–224 (2015).
14. Grashoff, C. *et al.* Measuring mechanical tension across vinculin reveals regulation of focal adhesion dynamics. *Nature* **466,** 263–266 (2010).
15. Huveneers, S. *et al.* Vinculin associates with endothelial VE-cadherin junctions to control force-dependent remodeling. *J. Cell Biol.* **196,** 641–652 (2012).
16. Yonemura, S., Wada, Y., Watanabe, T., Nagafuchi, A. & Shibata, M. α-Catenin as a tension transducer that induces adherens junction development. *Nat. Cell Biol.* **12,** 533–542 (2010).
17. Ishiyama, N. *et al.* An autoinhibited structure of α-catenin and its implications for vinculin recruitment to adherens junctions. *J. Biol. Chem.* **288,** 15913–15925 (2013).
18. Yao, M. *et al.* Force-dependent conformational switch of α-catenin controls vinculin binding. *Nat. Commun.* **5,** 4525; doi: 10.1038/ncomms5525 (2014).
19. Finer, J. T., Simmons, R. M. & Spudich, J. A. Single myosin molecule mechanics: piconewton forces and nanometre steps. *Nature* **368,** 113–119 (1994).
20. Oberhauser, A. F., Hansma, P. K., Carrion-Vazquez, M. & Fernández, J. M. Stepwise unfolding of titin under force-clamp atomic force microscopy. *Proc. Natl. Acad. Sci. USA* **98,** 468–472 (2001).
21. Popa, I., Kosuri, P., Alegre-Cebollada, J., Garcia-Manyes, S. & Fernández, J. M. Force dependency of biochemical reactions measured by single-molecule force-clamp spectroscopy. *Nat. Protoc.* **8,** 1261–1276 (2013).
22. Liu, R., Garcia-Manyes, S., Sarkar, A., Badilla, C. L. & Fernández, J. M. Mechanical characterization of protein L in the low-force regime by electromagnetic tweezers/evanescent nanometry. *Biophys. J.* **96,** 3810–3821 (2009).
23. Hoffmann, T. & Dougan, L. Single molecule force spectroscopy using polyproteins. *Chem. Soc. Rev.* **41,** 4781–4796 (2012).
24. Choi, H.-J. *et al.* αE-catenin is an autoinhibited molecule that coactivates vinculin. *Proc. Natl. Acad. Sci. USA* **109,** 8576–8581 (2012).
25. Maki, K., Han, S.-W. & Adachi, T. β-Catenin as a tension transmitter revealed by AFM nanomechanical testing. *Cell. Mol. Bioeng.* **8,** 14–21 (2015).
26. Lv, C. *et al.* Single-molecule force spectroscopy reveals force-enhanced binding of calcium ions by gelsolin. *Nat. Commun.* **5,** 4623; doi: 10.1038/ncomms5623 (2014).
27. Goldman, D. H. *et al.* Mechanical force releases nascent chain–mediated ribosome arrest *in vitro* and *in vivo*. *Science* **348,** 457–460 (2015).
28. Li, J. *et al.* Structural determinants of the mechanical stability of α-catenin. *J. Biol. Chem.* **290,** 18890–18903 (2015).
29. Thomas, W. A. *et al.* α-Catenin and vinculin cooperate to promote high E-cadherin-based adhesion strength. *J. Biol. Chem.* **288,** 4957–4969 (2013).
30. Pokutta, S., Drees, F., Takai, Y., Nelson, W. J. & Weis, W. I. Biochemical and structural definition of the l-afadin- and actin-binding sites of α-catenin. *J. Biol. Chem.* **277,** 18868–18874 (2002).

31. Yang, J., Dokurno, P., Tonks, N. K. & Barford, D. Crystal structure of the M-fragment of α-catenin: implications for modulation of cell adhesion. *EMBO J.* **20,** 3645–3656 (2001).
32. Cohen, D. M., Chen, H., Johnson, R. P., Choudhury, B. & Craig, S. W. Two distinct head-tail interfaces cooperate to suppress activation of vinculin by talin. *J. Biol. Chem.* **280,** 17109–17117 (2005).
33. Peng, X., Maiers, J. L., Choudhury, D., Craig, S. W. & DeMali, K. A. α-Catenin uses a novel mechanism to activate vinculin. *J. Biol. Chem.* **287,** 7728–7737 (2012).
34. Bois, P. R., O'Hara, B. P., Nietlispach, D., Kirkpatrick, J. & Izard, T. The vinculin binding sites of talin and α-actinin are sufficient to activate vinculin. *J. Biol. Chem.* **281,** 7228–7236 (2006).
35. Carrion-Vazquez, M. *et al.* Mechanical and chemical unfolding of a single protein: a comparison. *Proc. Natl. Acad. Sci. USA* **96,** 3694–3699 (1999).
36. Stirnemann, G., Giganti, D., Fernández, J. M. & Berne, B. J. Elasticity, structure, and relaxation of extended proteins under force. *Proc. Natl. Acad. Sci. USA* **110,** 3847–3852 (2013).
37. Bustamante, C., Marco, J. F., Siggia, E. D. & Smith, S. Entropic elasticity of lambda-phage DNA. *Science* **265,** 1599–1600 (1994).

Acknowledgements

This work was partly supported by CREST from JST, Japan, and by the Grant-in-Aid for Challenging Exploratory Research (15K13832) from the JSPS, Japan, and by the Platform Project for Supporting in Drug Discovery and Life Science Research (Platform for Dynamic Approaches to Living System) from the Ministry of Education, Culture, Sports, Science (MEXT) and Japan Agency for Medical Research and development (AMED), Japan. Koichiro Maki was supported by the JSPS Research Fellowships for Young Scientists.

Author Contributions

K.M., S.W.H. and T.A. designed and performed SMFS experiments. S.Y., Y.H. and T.H. constructed the samples and performed the biochemical characterizations. All authors contributed to data interpretation. K.M., S.Y., T.H. and T.A. contributed to manuscript preparation.

Additional Information

Supplementary information accompanies this paper at http://www.nature.com/srep

Competing financial interests: The authors declare no competing financial interests.

How to cite this article: Maki, K. *et al.* Mechano-adaptive sensory mechanism of α-catenin under tension. *Sci. Rep.* **6**, 24878; doi: 10.1038/srep24878 (2016).